Simultaneous evaluation of two branches of a multifunctional integrated optic chip with an ultra-simple dual-channel configuration

Yonggui Yuan,[1] Chuang Li,[1] Jun Yang,[1,*] Ai Zhou,[2] Shuai Liang,[1] Zhangjun Yu,[1] Bing Wu,[1] Feng Peng,[1] Yu Zhang,[1] Zhihai Liu,[1] and Libo Yuan[1]

[1]*Key Laboratory of In-fiber Integrated Optics of Ministry Education of China, Harbin Engineering University, Harbin 150001, China*

[2]*National Engineering Laboratory for Fiber Optic Sensing Technology, Wuhan University of Technology, Wuhan 430074, China*

**Corresponding author: yangjun141@263.net*

Received March 20, 2015; accepted March 24, 2015;
posted April 7, 2015 (Doc. ID 236376); published May 15, 2015

We propose an ultra-simple dual-channel configuration for simultaneously evaluating two branches of a multifunctional integrated optic chip (MFIOC). In the configuration, the MFIOC is employed as a beam splitter to construct the demodulation interferometer together with a 2×2 fiber coupler. Interference happens between polarization modes traveling through different channels of the MFIOC. The cross-couplings of each channel are respectively characterized by the interference peaks which distribute on opposite sides of the central interference peak. Temperature responses of the MFIOC are experimentally measured from –40°C to 80°C. Results show that the proposed configuration can achieve simultaneous dual-channel transient measurements with resolution of –90 dB and dynamic range of 90 dB. In addition, the two channels of the configuration have consistent measuring performance, and the two branches of the MFIOC have different responses to temperature variation.

OCIS codes: (120.3180) Interferometry; (120.2130) Ellipsometry and polarimetry; (120.3930) Metrological instrumentation.

http://dx.doi.org/10.1364/PRJ.3.000115

1. INTRODUCTION

The multifunctional integrated optic chip (MFIOC) is an important component for fiber-optic sensing applications [1–3] due to its multiple functions in beam splitting, optical polarization, and electro-optical phase modulation. A MFIOC is usually characterized with the polarization extinction ratio (PER) of the chip and local cross-couplings at connection points between the chip and its polarization maintaining (PM) pigtails. Accurately measuring these parameters is very important for fabrication and application of the MFIOC. Optical coherence domain polarimetry (OCDP) based on white light interferometry is a useful technique for measuring distributed polarization couplings in PM fibers [4–6] and optical devices [7]. It has been successfully used for one-channel evaluation of the MFIOCs [8–10].

In practical situation, there exists more or less difference between the two branches of the MFIOC. For some high-precision applications such as inertial measurement with fiber optic gyroscope (FOG) [11,12], the PER of the MFIOC is generally required to be higher than 80 dB. For such a high PER, a small difference, especially the transient response difference between the two branches of the MFIOC, will cause a significant impact on the performance such as random walk and zero drift of the FOG [13]. Therefore, for high-precision application, the difference of the parameters and their transient variation between the two branches of the MFIOC should be as small as possible. To obtain the transient response difference between the branches of the MFIOC, the two branches should be simultaneously evaluated. However, traditional OCDP method is just a single-channel testing configuration which cannot achieve two-branch simultaneous measurement. The full parameters of the MFIOC can only be obtained by evaluating one branch after the other, which means that two separate measurements are needed. In this case, the parameters of the two branches are not obtained simultaneously, and therefore the transient difference between the two branches cannot be accurately detected.

In this paper, we propose and demonstrate an ultra-simple dual-channel configuration for simultaneously evaluating the two branches of a MFIOC. Different from previous single-channel evaluation methods in which the MFIOC just is a device under test (DUT), the MFIOC in the present method acts not only as a DUT but also as an important component of the demodulation interferometer. The proposed configuration can accomplish simultaneous dual-channel evaluation with –90 dB resolution just using the same number of components as the single-channel configuration, which means that the ultra-simple configuration is cost effective and has high stability and reliability. To the best of our knowledge, this is the first time two branches of a MFIOC have been evaluated simultaneously.

2. SETUP AND ANALYSIS

The configuration of the dual-channel evaluating system is shown in Fig. 1. In the configuration, the beam splitting

function of the MFIOC is utilized to construct the demodulation Mach–Zehnder interferometer together with a 2×2 fiber coupler. The linearly polarized light output from the 45° rotated polarizer is launched into the lead-in pigtail of the MFIOC and split into its two branches. The orthogonal beams output from branch 1 transmit through the 45° rotated analyzer 1 and the optical path scanning mechanism. The beams output from branch 2 pass through the 45° rotated analyzer 2 and the polarization controller (PC). The beams from the two branches are finally combined by the 2×2 coupler and detected by the detectors. When the optical path length including branch 1 matches that including branch 2 by tuning the position of the scanning mirror, interference occurs. Different from the single-channel evaluation system in which the interference happens between the orthogonal polarization modes in the same fiber branch, in the present two-channel configuration, the modes in the same branch do not interfere, and the interference takes place between beams traveling along different branches. Therefore, for the single-channel configuration, the interference fringes arise in pairs and locate symmetrically around the central interference peak. Each pair of fringes corresponds to a cross-coupling point, and the parameters of the MFIOC can be obtained from the fringes on any side of the central peak. For the dual-channel configuration, the interference fringes do not appear symmetrically, and the fringes at different sides of the central peak present cross-coupling points in different paths.

For the sake of analysis, we use A, F, G, H, and I to represent the positions of the input polarizer, analyzer 1, analyzer 2, the scanning mirror, and the output coupler, respectively. The paths A-B-E-G-H-I and A-B-D-F-I are defined as path 1 and path 2, respectively. Points B, E, and D stand for the interfaces between the PM pigtails and the input end, output end 1, and output end 2 of the MFIOC, respectively. The cross-couplings at the interfaces are expressed as ρ_B, ρ_E, and ρ_D, respectively. The points a, e, and d denote the splice points between the pigtails of the MFIOC and the pigtails of the polarizer, analyzer 1, and analyzer 2, respectively. All the PM pigtails are spliced with 0° axis alignment, and the cross-couplings at these points are expressed as ρ_a, ρ_e, and ρ_d, respectively.

The light transmitting through the MFIOC demodulation configuration can be described with the Jones matrix method [10]. The light fields output from the analyzers 1 and 2 can be written as

$$\boldsymbol{E}_{\text{out1}} = \boldsymbol{T}_{\text{ana1}}\boldsymbol{T}_{45^\circ}\boldsymbol{T}_{f_{eG}}\boldsymbol{T}_{\rho_e}\boldsymbol{T}_{f_{Ee}}\boldsymbol{T}_{\rho_E}\boldsymbol{T}_Y\boldsymbol{T}_\xi\boldsymbol{T}_{\rho_B}\boldsymbol{T}_{f_{aB}}\boldsymbol{T}_{\rho_a}\boldsymbol{T}_{f_{Aa}}\boldsymbol{T}_{45^\circ}\boldsymbol{T}_{\text{pol}}\boldsymbol{E}_{\text{in}}, \tag{1}$$

$$\boldsymbol{E}_{\text{out2}} = \boldsymbol{T}_{\text{ana2}}\boldsymbol{T}_{45^\circ}\boldsymbol{T}_{f_{dF}}\boldsymbol{T}_{\rho_d}\boldsymbol{T}_{f_{Dd}}\boldsymbol{T}_{\rho_D}\boldsymbol{T}_Y\boldsymbol{T}_\zeta\boldsymbol{T}_{\rho_B}\boldsymbol{T}_{f_{aB}}\boldsymbol{T}_{\rho_a}\boldsymbol{T}_{f_{Aa}}\boldsymbol{T}_{45^\circ}\boldsymbol{T}_{\text{pol}}\boldsymbol{E}_{\text{in}}, \tag{2}$$

where $\boldsymbol{T}_{\text{pol}}$, $\boldsymbol{T}_{\text{ana1}}$, and $\boldsymbol{T}_{\text{ana2}}$ are transfer matrices of the polarizer and analyzers 1 and 2, respectively; $\boldsymbol{T}_{45^\circ}$ is the matrix of the 45° rotation angle of the polarizers; $\boldsymbol{T}_{f_{Aa}}$, $\boldsymbol{T}_{f_{aB}}$, $\boldsymbol{T}_{f_{Dd}}$, $\boldsymbol{T}_{f_{dF}}$, $\boldsymbol{T}_{f_{Ee}}$, and $\boldsymbol{T}_{f_{eG}}$ are transfer matrices of the PM pigtails with length of $\boldsymbol{l_{Aa}}$, $\boldsymbol{l_{aB}}$, $\boldsymbol{l_{Dd}}$, $\boldsymbol{l_{dF}}$, $\boldsymbol{l_{Ee}}$, and $\boldsymbol{l_{eG}}$, respectively; and $\boldsymbol{T}_{\rho_a}$, $\boldsymbol{T}_{\rho_B}$, $\boldsymbol{T}_{\rho_D}$, $\boldsymbol{T}_{\rho_d}$, $\boldsymbol{T}_{\rho_E}$, and $\boldsymbol{T}_{\rho_e}$ are transfer matrices of the coupling points a, B, D, d, E, and e, respectively; $\boldsymbol{T}_Y\boldsymbol{T}_\xi$ and $\boldsymbol{T}_Y\boldsymbol{T}_\zeta$ present the transfer matrices of branch 1 and branch 2 of the MFIOC, respectively, where $\xi{:}\zeta$ is the splitting ratio of the output coupler.

The output light fields $\boldsymbol{E}_{\text{out1}}$ and $\boldsymbol{E}_{\text{out2}}$ interfere at the coupler after transmitting through the optical path scanning mechanism and the PC, respectively. Neglecting the higher order terms of the interference signal, and only considering the constant and linear terms, the envelope of the interference signal can be expressed as

$$\begin{aligned}\frac{I(\tau)}{I(0)} &= R(\tau-\tau_1)+\rho_aR(\tau-\tau_1+\tau_{Aa})+\rho_BR(\tau-\tau_1+\tau_{AB})\\ &+\rho_ER(\tau-\tau_1+\tau_{EG})+\rho_eR(\tau-\tau_1+\tau_{eG})+\varepsilon_1R(\tau-\tau_2+\tau_{AB})\\ &+\rho_aR(\tau-\tau_1-\tau_{Aa})+\rho_BR(\tau-\tau_1-\tau_{AB})+\rho_DR(\tau-\tau_1-\tau_{DF})\\ &+\rho_dR(\tau-\tau_1-\tau_{dF})+\varepsilon_2R(\tau-\tau_3-\tau_{AB}),\end{aligned} \tag{3}$$

where $R(\tau)$ is the autocorrelation function of the light source; ε_1 and ε_2 are PERs of branch 1 and branch 2 of the MFIOC, respectively; and τ_{Aa}, τ_{AB}, τ_{EG}, τ_{eG}, τ_{DF}, and τ_{dF} are time-delay differences between two polarization modes in PM fibers of $l_{Aa}, l_{AB}, l_{EG}, l_{eG}, l_{DF}$, and l_{dF}, respectively. τ_1, τ_2, and τ_3 are time delay differences between beams transmitting along different paths, which are written as

$$\tau_1 = t_{n_x}^{BE}+t_{n_x}^{EG}+t_{n_0}^{GH}+t_{n_0}^{HI}-t_{n_x}^{BD}-t_{n_x}^{DF}-t_{n_0}^{FI}, \tag{4}$$

$$\tau_2 = t_{n_y}^{BE}+t_{n_y}^{EG}+t_{n_0}^{GH}+t_{n_0}^{HI}-t_{n_x}^{BD}-t_{n_x}^{DF}-t_{n_0}^{FI}, \tag{5}$$

$$\tau_3 = t_{n_x}^{BE}+t_{n_x}^{EG}+t_{n_0}^{GH}+t_{n_0}^{HI}-t_{n_y}^{BD}-t_{n_y}^{DF}-t_{n_0}^{FI}, \tag{6}$$

where $t_{n_i}^{MN}$ ($M=B,E,G,H,D$ or F, $N=E,G,H,I,D$ or F, $i=x,y$, or 0) is transit time of the light in the waveguides between points M and N. For PM fibers, $n_x=n_{\text{slow}}^{\text{fiber}}$ and $n_y=n_{\text{fast}}^{\text{fiber}}$; for the MFIOC, $n_x=n_{\text{fast}}^{\text{chip}}$ and $n_y=n_{\text{slow}}^{\text{chip}}$; for single mode fiber, the refractive index is expressed as n_0.

In Eq. (3), the first item on the right-hand side denotes the central interference peak which serves as reference for getting the amplitude (cross talk) and location [optical path difference (OPD)] of other interference peaks. The second to sixth items present the cross-couplings at points a, B, E, and e and the PER of branch 1, respectively. The interference peaks corresponding to these items appear on the left side of the central interference peak. The last five items stand for the cross-couplings at points a, B, D, and d and the PER of branch 2, respectively, and their corresponding interference peaks arise on the right side of the central peak.

3. RESULTS AND DISCUSSION

A two-branch MFIOC was tested by using the proposed dual-channel configuration as shown in Fig. 1. The light source used in the experiment is a superluminescent diode (PSDD1502, InPhenix, Inc., USA) with a central wavelength of 1550 nm and bandwidth of ~50 nm. The splitting ratio of the output coupler is 50:50. The circulator has 1 dB insertion loss and 55 dB return loss. The polarizer and analyzers have 30 dB PER and <1 dB insertion loss. The scanning mirror has a ~100 mm scanning range, >92% reflectivity, 1.5 dB insertion loss, and ±0.1 dB loss fluctuation. The photodetectors have a

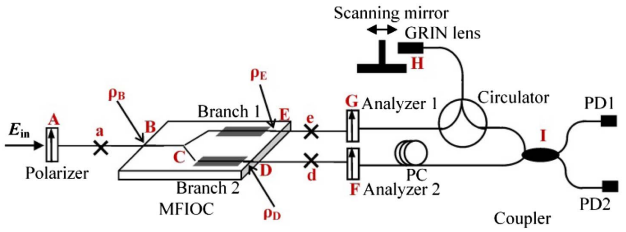

Fig. 1. Schematic diagram of the ultra-simple dual-channel configuration for simultaneously evaluating the MFIOC. GRIN, graded index.

working range of 1100–1700 nm and responsivity of >0.85. The lengths and estimated OPD of the PM pigtails and the tested MFIOC are presented in Table 1. The length and birefringence of the PM fibers and MFIOC are approximate values that are used for roughly estimating the OPD in each waveguide. According to these estimated OPDs, we can confirm the characteristic peak positions of the cross-coupling points and the PERs of the MFIOC.

The measured interference pattern of the MFIOC is shown in Fig. 2. The central peak corresponding to the first item of Eq. (3) is caused from the interference between the paths $AB_x \rightarrow BE_x \rightarrow EG_x$ and $AB_x \rightarrow BD_x \rightarrow DF_x$. The peaks on the left sides of the central peak represent the cross-coupling points in path 1, and those on the right side denote the cross-couplings in path 2. From the figure, the PER of the MFIOC is nearly −90 dB, and the dynamic range is about 90 dB, which are as high as those of the single-channel evaluation configuration [10].

The intensity and position of the characteristic peaks in Fig. 2 are shown in Table 2. Comparing the left peaks with

Table 1. Length and Estimated OPD of the MFIOC

MFIOC	Length (m)	Approximate Birefringence	Estimated OPD (mm)
l_{Aa}	19.0	5×10^{-4}	9.50
l_{aB}	1.22	5×10^{-4}	0.61
l_{BE}/l_{BD}	0.02	8×10^{-2}	1.60
l_{Ee}	1.20	5×10^{-4}	0.60
l_{Dd}	1.59	5×10^{-4}	0.80
l_{eG}	4.7	5×10^{-4}	2.35
l_{dF}	3.6	5×10^{-4}	1.80

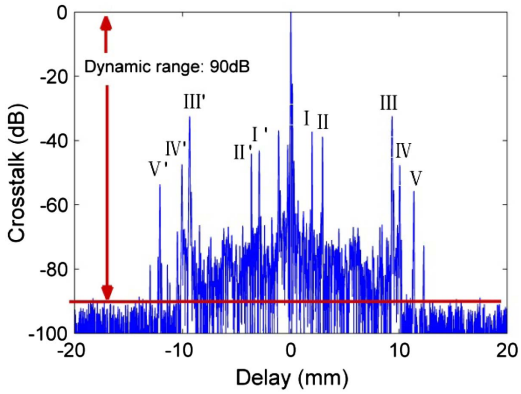

Fig. 2. Measured interference pattern of the MFIOC by using the dual-channel evaluating system. The left-side pattern expresses the cross-couplings of path 1, and the right-side pattern denotes the cross-couplings of path 2.

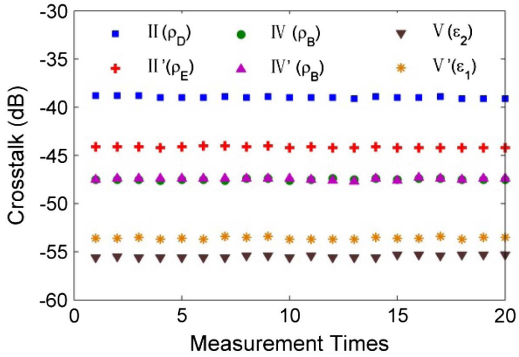

Fig. 3. Cross talk distribution of 20 measurements at room temperature.

the right ones, we can see that peaks III and IV have almost the same intensities as peaks III′ and IV′, respectively, whereas the intensities of peaks I, II, and V are quite different from those of peaks I′, II′, and *V′*, respectively. The nearly identical intensities between peaks III and III′ and peaks IV and IV′ verify the consistency between the performances of the two measuring paths. The differences in the other three peak pairs apparently indicate the difference between the two branches of the MFIOC. To verify the measurement repeatability of the two-channel configuration, the MFIOC was repeatedly measured 20 times at room temperature. The results are plotted in Fig. 3. The largest standard deviation of the crosstalk is 0.13 dB (3σ), which confirms that the evaluation system has good repeatability.

The MFIOC was then put into a temperature chamber to investigate the effect of temperature on the characteristics of the two branches of the MFIOC. The inconsistency of the temperature responses between the two branches can be directly obtained. In the experiment, the coupling points B, D, and E were in the temperature chamber, and points a, d, and e were out of the chamber. The temperature was increased from −40 to 80°C with a step of 5°C. The intensity variation of peaks II, II′, IV, IV′, V, and V′ are presented in Fig. 4. From the figure, we can see that intensities of peaks IV and IV′ which represent the cross talk at the same point B, have the same variation tendency. Such a phenomenon demonstrates that the two channels of the evaluating configuration have the same response to temperature variation. The fluctuation of the intensity of peak V′ (ε_1) is much smaller than that of peak V (ε_2), which indicates that branch 1 has better temperature stability than branch 2. The intensities of peaks II

Table 2. Measurement Results of the MFIOC

Peak	Position (mm)	Cross Talk (dB)	Corresponding Waveguide OPD
I (ρ_d)	1.962	−37.2	l_{dF}
I′ (ρ_e)	−2.924	−43.1	l_{eG}
II (ρ_D)	2.928	−38.8	l_{DF}
II′ (ρ_E)	−3.646	−44.1	l_{EG}
III (ρ_a)	9.362	−32.4	l_{Aa}
III′ (ρ_a)	−9.354	−32.5	
IV (ρ_B)	10.070	−47.5	l_{AB}
IV′(ρ_B)	−10.065	−47.5	
V(ε_2)	11.383	−55.7	$l_{AB}-l_{BD}+l_{DF}$
V′ (ε_1)	−12.098	−53.6	$l_{AB}-l_{BE}+l_{EG}$

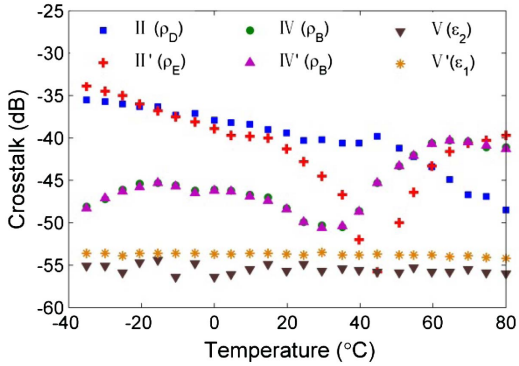

Fig. 4. Temperature responses of the two branches of the MFIOC.

(ρ_D) and II′ (ρ_E) change greatly with temperature variation, and the variation tendencies are quite different. The strong variations of ρ_D and ρ_E are due to the deformation of the optical adhesive for connecting the MFIOC and PM pigtails. The deformation of the adhesive will introduce stress on the PM pigtails and may cause slight rotation of the PM pigtails. Such temperature-caused stress and rotation mainly depend on the amount and shape of the adhesive; therefore the temperature response of the cross talks at the connections between the MFIOC and its pigtails is random for different MFIOCs.

4. CONCLUSIONS

In conclusion, we proposed an ultra-simple dual-channel configuration for simultaneously evaluating two branches of a MFIOC. We employed the MFIOC as a beam splitter to construct the demodulation interferometer. The beams transmitting through different branches of the MFIOC interfere with each other, and the characteristic peaks corresponding to each branch locate on opposite sides with respect to the central interference peak. The resolution and dynamic range of the dual-channel configuration are as high as –90 and 90 dB, respectively, which are comparable with those of the single-channel configuration. The temperature responses of the two branches were simultaneously measured, and results verify the simultaneous high-precision transient evaluation ability of the dual-channel configuration.

ACKNOWLEDGMENTS

This work was funded by the National Natural Science Foundation of China (Grants Nos. 61227013, 61307104, 61422505), the Program for New Century Excellent Talents in University (NCET-12-0623), the National Key Scientific Instrument and Equipment Development Project (No. 2013YQ040815), the Specialized Research Fund for the Doctoral Program of Higher Education (No. 20122304110022), and the Heilongjiang Provincial Natural Science Foundation (No. ZD201205).

REFERENCES

1. T. Findakly and M. Bramson, "High-performance integrated-optical chip for a broad range of fiber-optic gyro applications," Opt. Lett. **15**, 673–675 (1990).
2. N. Peng, Y. Huang, S. Wang, T. Wen, W. Liu, Q. Zuo, and L. Wang, "Fiber optic current sensor based on special spun highly birefringent fiber," IEEE Photon. Technol. Lett. **25**, 1668–1671 (2013).
3. Y. Yang, "Temperature sensor based on PNR in Sagnac interferometer," Chin. Opt. Lett. **2**, 259–261 (2004).
4. Z. Li, Z. Meng, X. Chen, T. Liu, and X. S. Yao, "Method for improving the resolution and accuracy against birefringence dispersion in distributed polarization cross-talk measurements," Opt. Lett. **37**, 2775–2777 (2012).
5. H. Zhang, Y. Ren, T. Liu, D. Jia, and Y. Zhang, "Self-adaptive demodulation for polarization extinction ratio in distributed polarization coupling," Appl. Opt. **52**, 4353–4359 (2013).
6. B. Wu, J. Yang, Y. Yuan, H. Lv, C. Liu, A. Zhou, and L. Yuan, "Performance tests of PM optical fiber coupler based on optical coherence domain polarimetry," Proc. SPIE **8421**, 8421A2 (2012).
7. H. Liu, R. Li, and J. Wang, "White light interferometry test and analysis of $LiNbO_3$ polarizer," Optik **124**, 3891–3894 (2013).
8. W. S. Choi and M. S. Jo, "Accurate evaluation of polarization characteristics in the integrated optic chip for interferometric fiber optic gyroscope based on path-matched interferometry," J. Opt. Soc. Korea **13**, 439–444 (2009).
9. C. Li, C. Zhang, X. Wang, L. Li, J. Yu, and X. Feng, "White light interferometery for pigtail polarization crosstalk of Ti-diffused $LiNbO_3$ integrated optic phase modulator," Chin. J. Lasers **40**, 0808003 (2013).
10. J. Yang, Y. Yuan, A. Zhou, J. Cai, C. Li, D. Yan, S. Huang, F. Peng, B. Wu, Y. Zhang, Z. Liu, and L. Yuan, "Full evaluation of polarization characteristics of multifunctional integrated optic chip with high accuracy," J. Lightwave Technol. **32**, 3641–3650 (2014).
11. H. C. Lefevre, *The Fiber-optic Gyroscope* (Artech House, 1993), Chap. 3.
12. S. Divakaruni and S. Sanders, "Fiber optic gyros: a compelling choice for high precision applications," in *Optical Fiber Sensors*, OSA Technical Digest (CD) (Optical Society of America, 2006), paper MC2.
13. B. Szafraniec and G. Sanders, "Theory of polarization evolution in interferometric fiber-optic depolarized gyros," J. Lightwave Technol. **17**, 579–590 (2014).